Focused Ultrasound Ablation for the Treatment of Patients With Localized Deformed Breast Cancer: Computer Simulation

Prempreeya Montienthong
Center of Excellence in Electromagnetic Energy Utilization in Engineering (C.E.E.E.),
Department of Mechanical Engineering,
Faculty of Engineering,
Thammasat University,
(Rangsit Campus), 99 Moo 18,
Klong Luang, Pathumthani 12120, Thailand
e-mail: monprempreeya@gmail.com

Phadungsak Rattanadecho
Center of Excellence in Electromagnetic Energy Utilization in Engineering (C.E.E.E.),
Department of Mechanical Engineering,
Faculty of Engineering,
Thammasat University,
(Rangsit Campus), 99 Moo 18,
Klong Luang, Pathumthani 12120, Thailand
e-mail: ratphadu@engr.tu.ac.th

This paper is carried out on the computer simulation of breast cancer treated using a high intensity focused ultrasound (HIFU). The mathematical models consist of the pressure acoustics equation, bioheat equation, heat transfer in a blood vessel, momentum equations in a blood vessel, and mechanical deformation equation. In the numerical simulation, these mathematical models are solved by using an axisymmetric finite element method (FEM) with time-dependent, thermal and acoustic properties to describe the temperature distribution and the total displacement in tissue. The comparison of the simulated results in the model with two sizes of the cancer tumor and two frequencies of ultrasound are also considered in order to approach realistic tissue modeling. The results show that the breast cancer model with deformation, which is the more accurate way to simulate the physical characteristics of therapeutic breast cancer compared to the literature results, hence leads to more useful in the medical approach and this study was conducted to prevent errors caused by inaccurate focal points. [DOI: 10.1115/1.4044393]

Keywords: breast cancer treatment, deformed breast cancer, focused ultrasound ablation, bioheat, the total displacement in tissue

1 Introduction

Over the years, cancer has grown into deadly infection and leads to the majority of deaths around the world. According to The World Health Organization (WHO), the global burden of cancer has doubled since last 30 years, which will further double by 2020 and triple by 2030 [1]. Cancer once commonly identified in westernized and industrialized countries has now become a common disease of low- and medium-resource countries [2].

Breast cancer is a major health concern in the community and an important cause of cancer death in women. Surgical breast cancer treatment is effective but is a highly invasive procedure especially for the treatment of early diagnosed cancers (small tumors). Therefore, the need for minimally invasive techniques in the treatment of breast cancer has increased in recent years.

High intensity focused ultrasound (HIFU) is a treatment that aims to kill cancer cells with high-frequency sound waves. HIFU does not pass through bones or solid air, so it is not suitable for all types of cancer. These waves deliver a strong beam to a specific part of cancer. Some cells die when this high-intensity ultrasound beam is focused directly onto them. HIFU is only useful to treat a single tumor or part of a large tumor. It cannot be used to treat tumors that are more widespread. This means that HIFU is not suitable for people with cancer that has spread to more than one place in their body. HIFU has been successfully used as a new technique for treating tumors in clinical application [3,4]. Although other methods of thermal ablation such as the laser, microwave, and HIFU are being performed, HIFU is currently receiving the greatest attention in the light of several factors: its general availability, the recent technical advances help facilitate the use and aggressive marketing of cancer. HIFU Treatment is a revolutionary, minimally invasive radiation-free treatment for patients with localized breast cancer or tumor. Ultrasound energy does not cause harm to any tissue surrounding the targeted focal points. Advantages of HIFU Treatment are no blood loss, nonsurgical, radiation-free, quick recovery, and an outpatient procedure. Ultrasound has been used for a variety of therapeutic applications including muscle diathermy and bone healing [5], controlling drug release [6,7], and mild hyperthermia [8–10] Ultrasound exposure has been shown to reduce smooth muscle cell proliferation in vitro [11]. Focused ultrasound ablation is highly attractive because of wide acceptance of ultrasound in medicine, easy and accurate focusing to the deeply seated organs in the body, high efficiency in perturbing cell membranes and increasing their permeability, noninvasiveness, nonviral nature, low cost, and nonionization for theoretically unlimited treatment [12]. Therefore, the numerical analysis of heat transfer in breast cancer exposed to focused ultrasound ablation will provide useful information on the absorption of pressure acoustic energy, temperature distribution, and the total displacement under a variety of exposure conditions. The thermal modeling of breast cancer tissue is important as a tool to investigate the effect of external heat sources, and to predict abnormalities in tissues, for example, expanding of tissue. However, in real situations, the temperature cannot be measured directly in the human body but must be found indirectly through numerical techniques.

There are some experimental studies of temperature in animals, such as in rats, cows, and pigs [13,14]. However, the results may not represent the practical transport processes that occur in human tissues. Calculating the electromagnetic field, the pressure acoustics energy, total displacement distribution, and the temperature distribution become more complex when the human body is nonuniform in shape and contains several organs or tissues. Our research group and other groups have numerically investigated the temperature distribution in porous tissue and human tissue subjected to the electromagnetic field in different situations. For example, Montienthong et al. [15] studied the distributions of solid and fluid temperatures, concentration, and flow field within a porous media under electromagnetic wave and investigated based on the local thermal nonequilibrium model. Wessapan and Ratanadecho [16] carried out a three-dimensional human head model, which was used to simulate the SAR distribution and the temperature distribution over the human head at different geometry. The results show that the maximum temperature increase in the skin of an adult head is higher than that of child head. While the maximum temperature increase in the brain of an adult head is

Contributed by the Heat Transfer Division of ASME for publication in the Journal of Heat Transfer. Manuscript received January 22, 2019; final manuscript received June 28, 2019; published online September 13, 2019. Assoc. Editor: Bumsoo Han.

lower than that of child head. Moreover, it is found that the temperature distributions in human head induced by mobile phone radiation are not directly related to the SAR distribution, due to the effects of dielectric properties, thermal properties, blood perfusion, and penetration depth of the electromagnetic power. Klinbun and Rattanadecho [17] carried out numerically the heating of multilayer porous packed bed, which is subjected to the microwave radiation with a rectangular waveguide. Wessapan and Ratanadecho [18] carried out the simulation of the SAR distribution and temperature distribution in an anatomically human eye exposed to electromagnetic field based on porous media theory. Wessapan et al. [19] carried out a two-dimensional human cross section model, which was used to simulate the SAR distribution and temperature distribution over the human body at different frequencies. Wongchadakul et al. [20] developed the thermal mechanical deformation model of skin during laser-induced thermotherapy based on a three-layered skin model. Manenti et al. [21] studied and compared the efficacy of radiofrequency ablation and Cryoablation in the treatment of early breast cancer. Quaranta et al. [22] evaluated the efficacy of cool-tip electrode RF breast ablation in terms of temperature distribution and duration of the procedure as compared with conventional multiprobe RF breast ablation. Hipp et al. [23] used a clinical MR-HIFU platform designed for treatment of uterine fibroids, tissue-mimicking phantoms, and ex vivo tissue to evaluate limitations and safety concerns of wave reflections from a reflective medium. Yang et al. [24] evaluated the effect of high-intensity focused ultrasound (HIFU) on subcutaneous murine neuroblastoma C1300. HIFU treatment was administered with a focused 4-MHz quartz transducer with a peak intensity of 550 W/cm^2. In experiment, 60 animals with tumor were divided into four groups. All the animals received a second tumor challenge in the right flank. Reduced tumor growth following a second tumor challenge was demonstrated in group IA as compared with other groups ($P < 0.001$), implying a stimulation of host tumor immunity following curative HIFU treatment. The data suggest that HIFU may be an alternative modality for the treatment of unresectable neuroblastoma. The first clinical application of HIFU was the use of extracorporeal shockwave lithotripsy as a method for treating kidney stones and due to the development of modern technology and advanced imaging methods, interest in HIFU was revived in the 1990s, realizing that it can produce instant cell death to the focused areas of tissue. Currently, HIFU has been used in the treatment of both benign and malignant tumors in the liver, breast kidney, uterine, and prostate [25,26].

This study considers the computationally determined the acoustic pressure field, intensity magnitude, temperature distribution, and the total displacement distribution in the breast cancer tissue exposed to the focus ultrasound ablation. Much attention is paid to the effects of the ultrasound frequency and size of tumor on the acoustic pressure field, the intensity magnitude, temperature distribution, and the total displacement distribution induced by exposure to focused ultrasound ablation obtained through numerical simulation of the pressure acoustics, Pennes' bioheat equation, stress–stain equation, the momentum equations, and heat transfer in blood vessel. The work described in this paper extended from previous work by further enhancing the focus on the effect of the expand breast cancer tissues and total displacement distribution under the focus ultrasound ablation. This computer simulation is indispensable to preplanning treatment application in order to prevent injury from unwanted thermal.

2 Formulation of the Problem

According to the real biological structure, the breast cancer tissue is divided into three layers: the fat, the glandular, and the muscle [1]. In a realistic situation, when the breast cancer tissue is exposed to ultrasound ablation, deformation is occurred at the heated positions due to the temperature distribution. In this work, a two-dimension axisymmetric thermomechanical breast cancer tissue model is used to study phenomena that occur in the tissue layer during subjected to ultrasound ablation. The absorption characteristics and phenomena occurred in breast cancer tissue depend on a number of factors, including the thermal properties of breast cancer tissues, and acoustic properties, as shown in Tables 1 and 2, respectively.

Table 1 The thermal properties of the breast cancer tissues [1]

Breast tissue layers	h	c	k	ρ	ω_b	Q'''_{met}
Fat	5	3000	0.21	920	0.1796×10^{-3}	400
Glandular	45	3000	0.48	1080	5.3908×10^{-4}	700
Muscle	15	3800	0.48	1085	5.3908×10^{-4}	700
Blood	—	4200	0.501	1060	—	—

Table 2 The acoustic properties of breast and cancerous tissues [1]

Breast tissue layers	c_c (speed of sound)	α at 1 MHz	α at 1.5 MHz	η
Fat	1479 ± 32	0.158	0.2098	1.7
Glandular	1553 ± 35	0.870	1.0655	1.5
Muscle	1545 ± 5	1.09	1.2819	1.4
Blood	1540	0.1303	0.1532	1.4

2.1 Analysis of the Pressure Acoustics, Frequency Domain. Ultrasound is a mechanical vibration of matter with a frequency above the audible range (more than 20 kHz). The wave is propagating through the medium as a disturbance of the particles in the medium supporting the wave. Particles will oscillate around their mean positions in a 3D manner, in general, liquids, soft tissue, and gas production only longitudinal waves. The factors of acoustic impedance are properties of the wave of the object that the wave is progressing through. Ultrasound wave propagating in the breast cancer tissue will be attenuated because of absorption and scattering.

The mathematical models illustrate the pressure acoustics and its variations and relate them to the physiological phenomena that arise from the interactions between focused ultrasound ablation and biological tissues. To simplify the problem, the following assumptions are made:

(1) The pressure acoustics is modeled in two dimensions.
(2) The focused ultrasound interaction with the tissue proceeds in the open region.
(3) The free space is truncated by a scattering boundary condition.
(4) The model assumes that the acoustic properties of each tissue are constant.

To describe the ablation of focused ultrasound through a tissue, the focused ultrasound ablation is calculated using the pressure acoustics, which mathematically describes the interdependence of the focused ultrasound ablation. The general form of the pressure acoustics is simplified to demonstrate the focused ultrasound ablation that into the breast cancer tissue as follows:

The pressure acoustics, frequency domain [27]

$$\nabla \cdot \left(-\frac{1}{\rho_c}(\nabla p_t - q_d) \right) - \frac{k_{\text{eq}}^2 p_t}{\rho_c} = Q_m \tag{1}$$

$$k_{\text{eq}}^2 = \left(\frac{\omega}{c_c}\right)^2 - \left(\frac{m}{r}\right)^2 \tag{2}$$

$$c_c = \frac{\omega}{k}, \quad k = \frac{\omega}{c} - i\alpha, \quad \rho_c = \frac{\rho c^2}{c_c^2} \tag{3}$$

p_t is the acoustic pressure (N/m^2), ω is the angular frequency (rad/s) c_c is speed of sound (m/s), q_d is the dipole source term (W/m^3), Q_m is the monopole source term (W/m^3), α is the acoustic

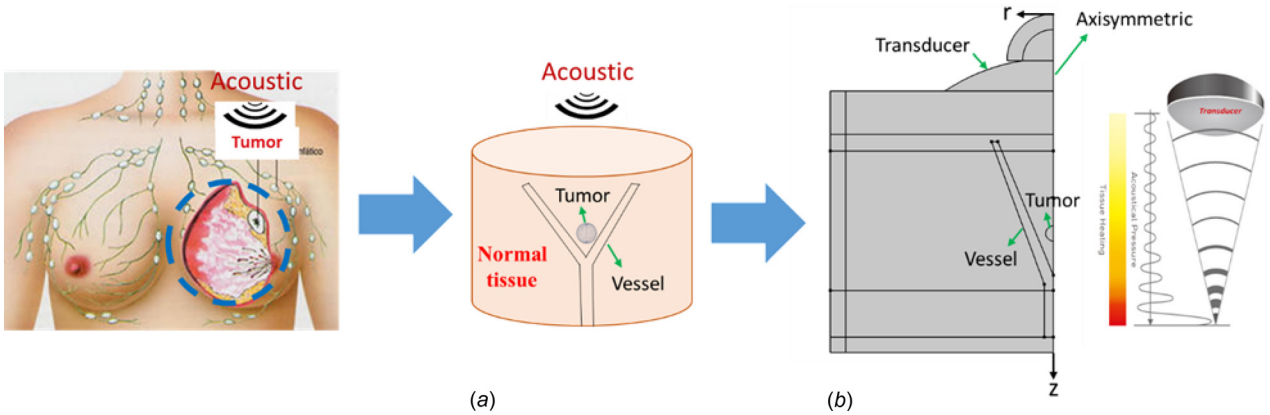

Fig. 1 The breast cancer tissue model: (*a*) three-dimensional breast cancer tissue model with ultrasound ablation and (*b*) two-dimensional breast cancer tissue model with ultrasound ablation: (*a*) 3D domain and (*b*) 2D axisymmetric domain

attenuation coefficient in the breast tissue and the vessel (dB/cm MHz).

In this study, the dipole source term and the monopole source term assumed to be zero.

The boundary condition for the pressure acoustics, frequency domain as below

$$\text{Sound hard boundary wall} \quad -n\cdot\left(-\frac{1}{\rho_c}(\nabla p_t - q_d)\right)=0 \qquad (4)$$

$$\text{Intensity determined} \quad I=\frac{Q_m}{2\alpha}$$

2.2 Analysis of the Heat Transfer in Breast Cancer Tissue. To solve the thermal problem, the coupled effects of the pressure acoustics propagation and the unsteady bioheat transfer are investigated. The temperature distribution corresponds to the thermal properties of breast cancer tissue. The absorbed energy from the mechanical wave (acoustic pressure) is converted to thermal energy, which increases the tissue temperature. To reduce the complexity of the problem, the following assumptions are made:

In order to simulate the breast cancer ablation, a model of unsteady heat transfer, as well as boundary conditions, is investigated. Heat transfer analysis on the tissue during breast cancer ablation is modeled in a 2D tissue thermomechanical model constructed in an axis symmetric plane. To simplify the problem, the following assumptions are made:

(1) The breast cancer tissue is a bio-material with constant thermal properties in the same layer.
(2) There is no phase change of substance in the breast cancer tissue.
(3) There is no chemical reaction in the breast cancer tissue.
(4) The two-dimensional model with an axisymmetric plane is assumed.
(5) Unsteady heat transfer is considered.
(6) The contact surface between each tissue is assumed to be a smooth condition.
(7) All the breast cancer tissues are assumed to be homogeneous and isotropic.

The modeling of heat transport in tissue was first introduced by Pennes based on the heat diffusion equation. The equation is normally called Pennes' bioheat equation and it is frequently used for the analysis of heat transfer in human tissues. Due to simplifications of the Pennes' bioheat model, other researchers have established mathematical bioheat model by extending or modifying the Pennes' bioheat model [28–30]. Although many advanced transport models of biological tissue have been proposed, Pennes' bioheat model is still a good approximation and it is still widely used for modeling the heating of biological tissue because of its easy implementation and its minimal data requirement.

The temperature increase in the breast cancer tissue is obtained by solving Pennes' bio-heat equation [31,32]. The transient bioheat equation effectively describes how heat transfer occurs within the breast cancer tissue, and the equation can be written as:

Pennes' Bioheat Equation

$$\rho C\frac{\partial T}{\partial t}=\nabla\cdot(k\nabla T)+\rho_b C_b\omega_b(T_b-T)+Q_{\text{met}}+Q_{\text{ext}} \qquad (5)$$

where ρ is the tissue density (kg/m^3), C is the heat capacity of the tissue (J/kg K), k is the thermal conductivity of the tissue (W/m K), T is the tissue temperature (°C), $\rho_b C_b\omega_b(T_b-T)$ is a source term accounting for blood perfusion, T_b is the temperature of the blood (°C) assumed to equal 36 °C, ρ_b is the density of the blood (kg/m^3), C_b is the heat capacity of the blood (J/kg K), ω_b is the blood perfusion rate (1/s), Q_{met} is the metabolic heat source (W/m^3) neglected since it is small, and Q_{ext} is the external heat source (the acoustic pressure heat source) (W/m^3). Tables 1 and 2 show the acoustic and thermal properties of the breast cancer tissues used in the simulations.

Because the general heat transfer application in COMSOL does not include the thermal effects of perfusion included in the Pennes' bioheat equation, the effects of perfusion were simulated in the muscle and fat tissues using the external heat source term (Q_{ext}), which is equal to the resistive heat generated by the ultrasound ablation.

The boundary condition for the heat transfer analysis: It is assumed that no contact resistance occurs between the internal tissues of the breast cancer. Therefore, the internal boundaries are assumed to be continuous. The heat transfer analysis excludes the surrounding space and is considered only in the breast cancer tissue model. The breast cancer tissue, as shown in Fig. 1, is considered under the constant boundary condition, At the initial stage, the temperature distribution within the breast cancer tissue is assumed to be uniform at 36 °C. Therefore, the temperature boundary condition of 36 °C is applied to all the surface boundaries. The initial temperature of skin tissue is 36 °C.

2.3 Analysis of Mechanical Deformation. In this study, breast cancer tissue is considered an isotropic material. The physical problem of solid mechanics for axisymmetric geometry can be described mathematically using the equilibrium equation, the stress–strain relationship, and the strain displacement relationship as follows:

Stress–stain equation

$$\frac{\partial\sigma_{rr}}{\partial r}+\frac{\partial\sigma_{rz}}{\partial z}+\frac{\sigma_{rr}-\sigma_{\varphi\varphi}}{r}+F_r=0 \qquad (6)$$

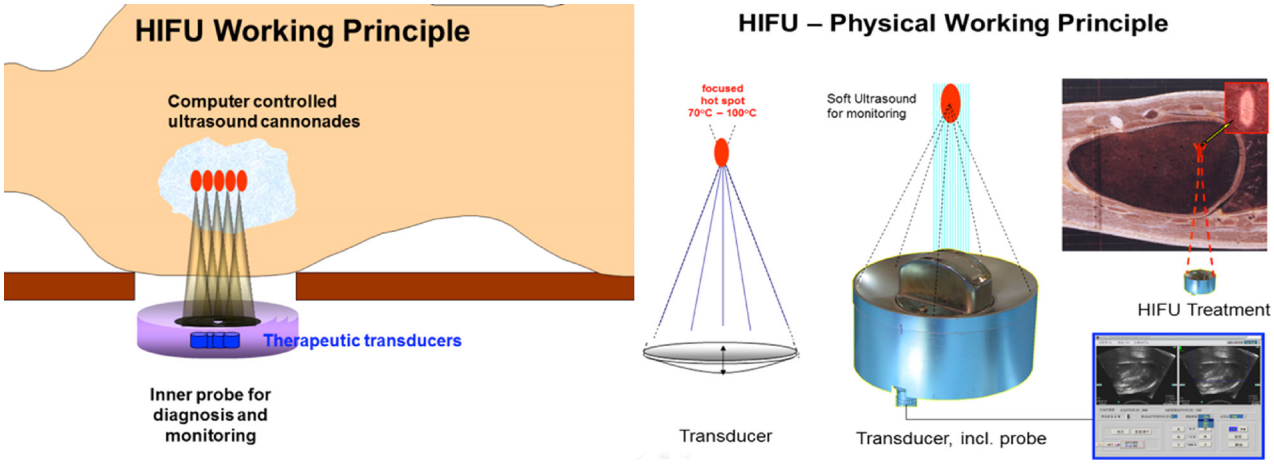

Fig. 2 Treating a patient with HIFU

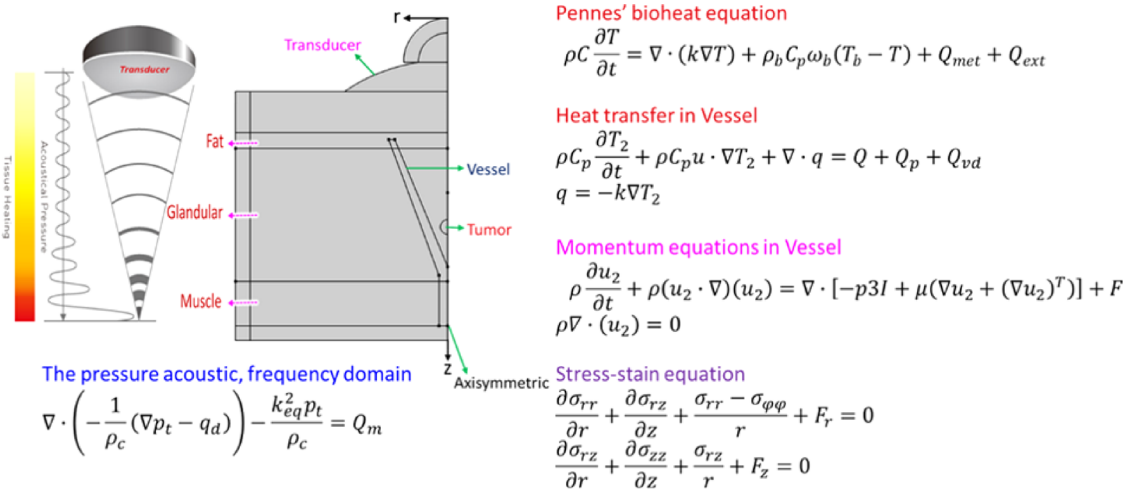

Fig. 3 Computational model: Axis symmetrical model geometry and physical domain

$$\frac{\partial \sigma_{rz}}{\partial r} + \frac{\partial \sigma_{zz}}{\partial z} + \frac{\sigma_{rz}}{r} + F_z = 0 \tag{7}$$

where σ in Eqs. (6) and (7) denotes the stress (Pa), F_r is the external body load (0 here).

In this study, the boundary condition for the mechanical deformation analysis is assumed to be free for all surfaces. The tissue is deformed as an effect of thermal strain. In addition, the initial stress and strain are set to zero.

$$\sigma_{ri},\ \sigma_{\varphi i},\ \sigma_{zi} \quad \text{and} \quad \sigma_{rzi} = 0\,\text{Pa}\,(\text{N/m2}) \tag{8}$$

$$\varepsilon_{ri},\ \varepsilon_{\varphi i},\ \varepsilon_{zi} \quad \text{and} \quad \varepsilon_{rzi} = 0 \tag{9}$$

where ε in Eq. (9) denotes the strain (Pa).

2.4 Analysis of the Momentum Equations in Blood Vessel. This study models the blood vessel flow in the relative blood vessel within the breast cancer using the continuity and momentum equations for the laminar and incompressible blood vessel flow and can be written.

The momentum equations in blood vessel

$$\rho \frac{\partial u_2}{\partial t} + \rho (u_2 \cdot \nabla)(u_2) = \nabla \cdot \left[-p3I + \mu\left(\nabla u_2 + (\nabla u_2)^T\right)\right] + F \tag{10}$$

$$\rho \nabla \cdot (u_2) = 0 \tag{11}$$

Here, u_2 represents the blood vessel velocity, p is the pressure, ρ is the blood density, F is the prescribed body force per unit volume

$F =$ Gravity is a body force that acts in the negative z-direction.

$F = \rho_b g$

where μ is the dynamic viscosity.The initial velocity field v_0 is assumed to be divergence-free.

To reduce the complications of the problem, the following assumptions are applied that velocity flow in blood vessel is constant. The boundary condition for the momentum equations in blood vessel: normal inflow and outflow velocity are 6.8 m/s, initial velocity = 0, $p = 90$ mmHg [33] and no-slip boundary condition are applied at all the walls.

2.5 Analysis of the Heat Transfer Equation in Blood Vessel. Heat transfer in blood vessel

$$\rho C_p \frac{\partial T_2}{\partial t} + \rho C_p u \cdot \nabla T_2 + \nabla \cdot q = Q + Q_p + Q_{vd} \tag{12}$$

$$q = -k \nabla T_2 \tag{13}$$

T_2 represents the blood vessel temperature and $Q + Q_p + Q_{vd}$ is the volumetric heating of blood volume due to external source.

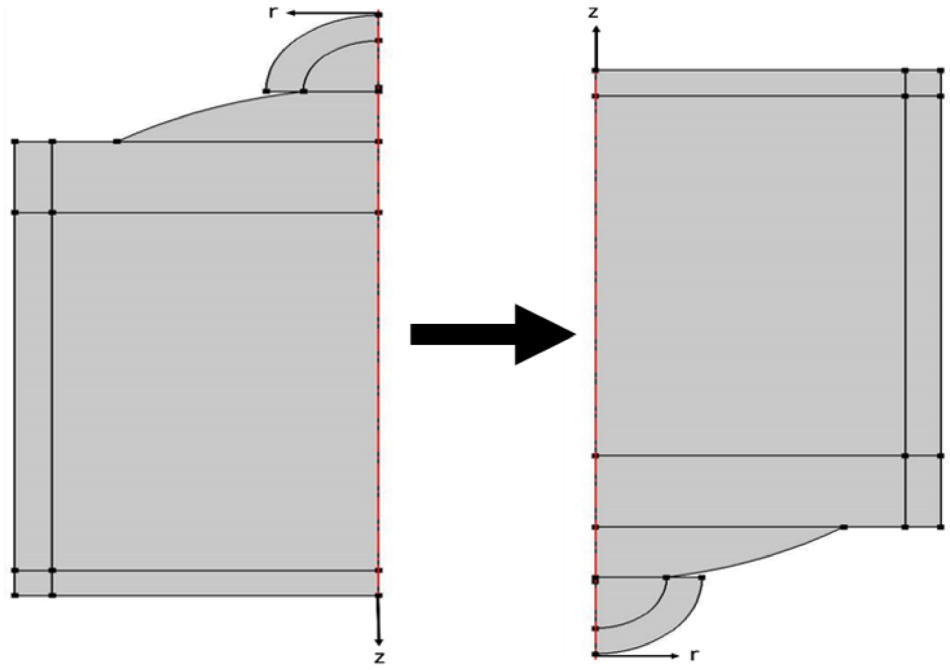

Fig. 4 Computational model of breast cancer tissue upside down model

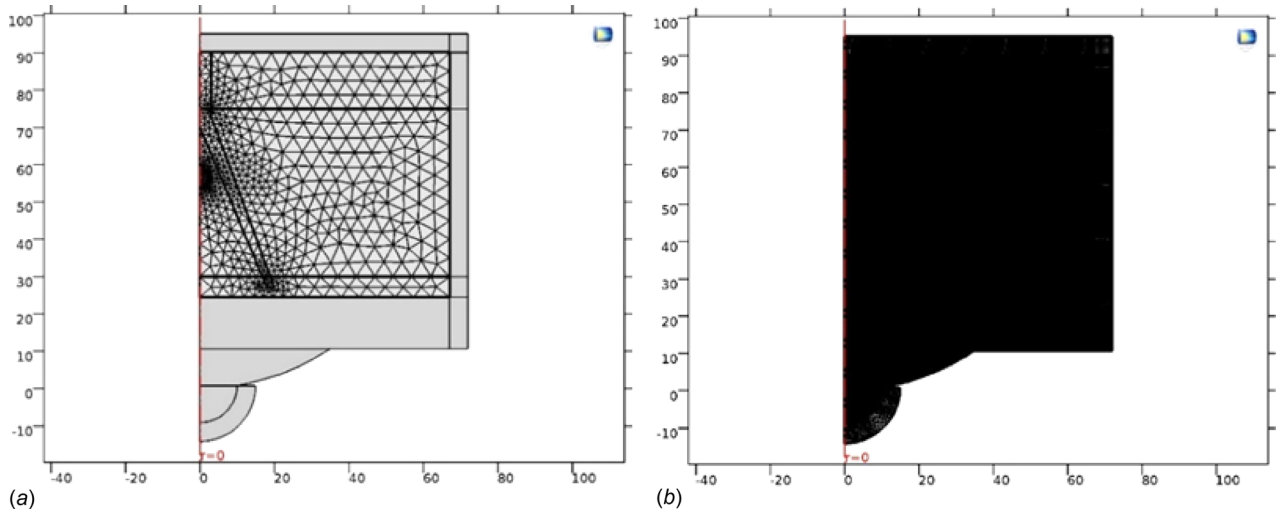

Fig. 5 The two-dimensional finite element mesh of breast cancer model: (*a*) bioheat equation, heat transfer, momentum equations in vessel, and mechanical deformation equation and (*b*) the pressure acoustics equation

The boundary condition for the heat transfer equation in blood vessel

The constant temperature at all boundary is 36 °C, and the initial temperature is 36 °C.

3 Method and Model

In this study, the frequencies of 1.0 and 1.5 MHz are chosen. As these frequencies are used globally in a wide range of applications, ultrasound ablation was simulated in breast cancer tissue models, using the finite element (FEM) method. The resulting ultrasound power accumulation patterns were used as a heat source for the Pennes' bioheat equation in a COMSOL® Multiphysics heat transfer model. To sufficiently explain the biological effects, which are associated with the ultrasound ablation, a systematic study of ultrasound ablation distribution patterns that interact with tissues is necessary. Therefore, this study presents the computational determination of the acoustic pressure and temperature distribution in the breast cancer tissue exposed to the focus ultrasound ablation. The breast cancer model comprises five types of tissue viz., fat, glandular, muscle, blood vessel, and tumor. The study focuses attention on temperature distribution and mechanical deformation induced in the breast cancer tissue subjected to focused ultrasound ablation in different situations. The FEM numerical simulation via COMSOL™ Multiphysics is applied to model the temperature distribution and deformation of breast cancer tissue. The phenomenon of ultrasound in the breast cancer tissue is described using the pressure acoustics.

3.1 Physical Model. A two-dimension axisymmetric breast cancer model is employed to determine the temperature distribution and deformation within the breast cancer tissue during ultrasound ablation process. Fig. 2[1] shows treating a patient with

[1]http://www.biomaxx-holding.com/HIFU.php

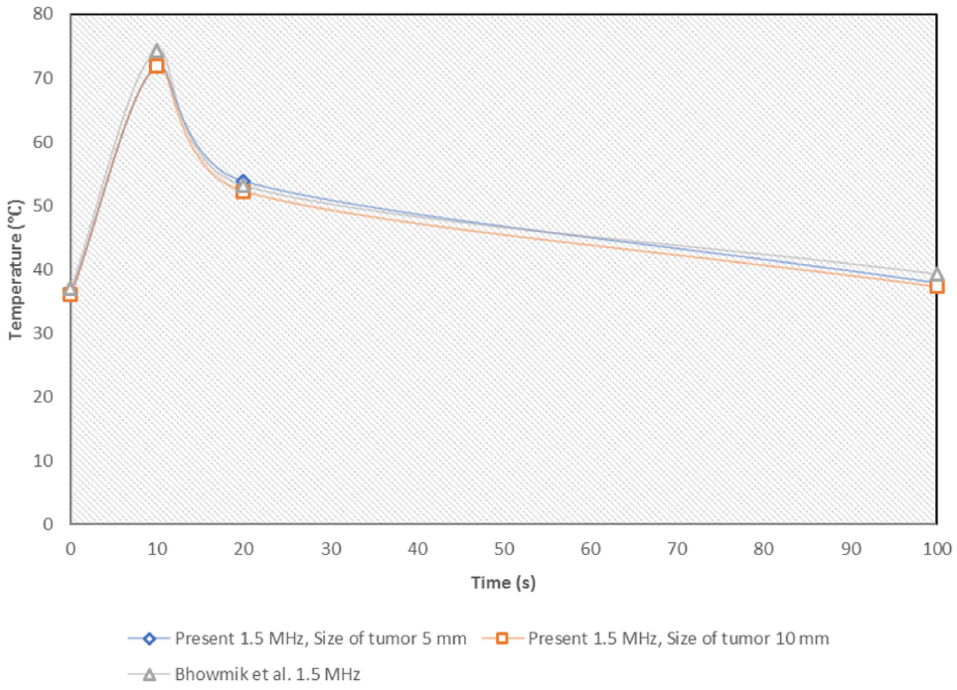

Fig. 6 Verification of the calculated temperature distribution to the temperature distribution obtained by Bhowmik et al. [1]

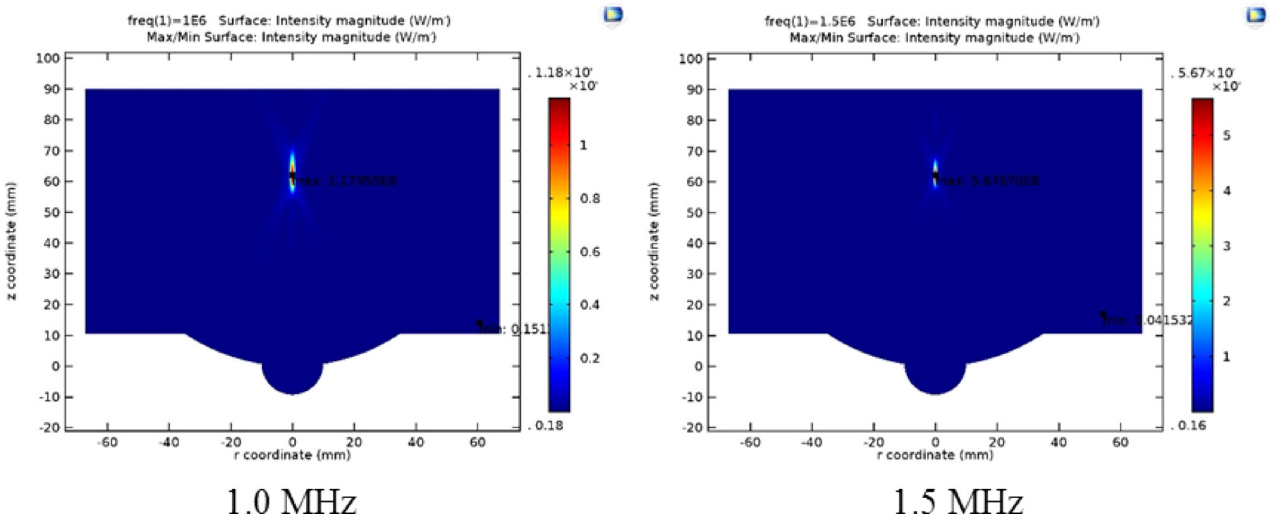

Fig. 7 The intensity magnitude at frequency of 1.0 and 1.5 MHz, size of tumor of 5 mm at ablation time of 10 s

HIFU. Fig. 1 shows the 3D and 2D of the breast cancer tissue model with focused ultrasound ablation used in this study.

Although the breast cancer tissue comprises of complex heterogeneous tissue, the model used in this study was assumed and constructed in an axisymmetric plane with three distinct layers viz., fat, glandular, and muscle tissue, as shown in Fig. 3, that shows the computational model: axis symmetrical model geometry, and physical domain used in this study. To simplify the problem, these layers are assumed to be homogeneous, uniform, and isotropic in the same layer, which means there is no difference in the thermal and acoustic properties within any layer. The focused ultrasound ablation to the surface has a portion of the mechanical vibration at the breast tissue. The acoustic and thermal properties of breast cancer tissues are given in Tables 1 and 2. Figure 4 shows the computational model of breast cancer tissue upside down model. Figure 5 shows the two-dimensional finite element mesh of breast cancer model. (a) Bioheat equation, heat transfer, momentum equations in blood vessel, and mechanical deformation equation and (b) The pressure acoustics equation.

4 Results and Discussion

Currently, HIFU has been used in the treatment of both benign and malignant tumors in the liver, breast, kidney, uterine, and prostate [25]. In HIFU, a wave propagates from the transducer through the different tissue layers toward the target site (Fig. 2). A part of the energy carried by the sound wave is reflected every time the ultrasound wave reaches a tissue boundary, while the remaining energy will pass through the tissue layer. The amount of energy that passes through is dependent on the density of the tissue, the speed of sound within tissue layers, and the thickness of the tissue layers. It is, therefore, important to minimize the effect of reflection at the tissue boundaries, as it will otherwise not be feasible to reach the target [25,34]. When an ultrasound wave

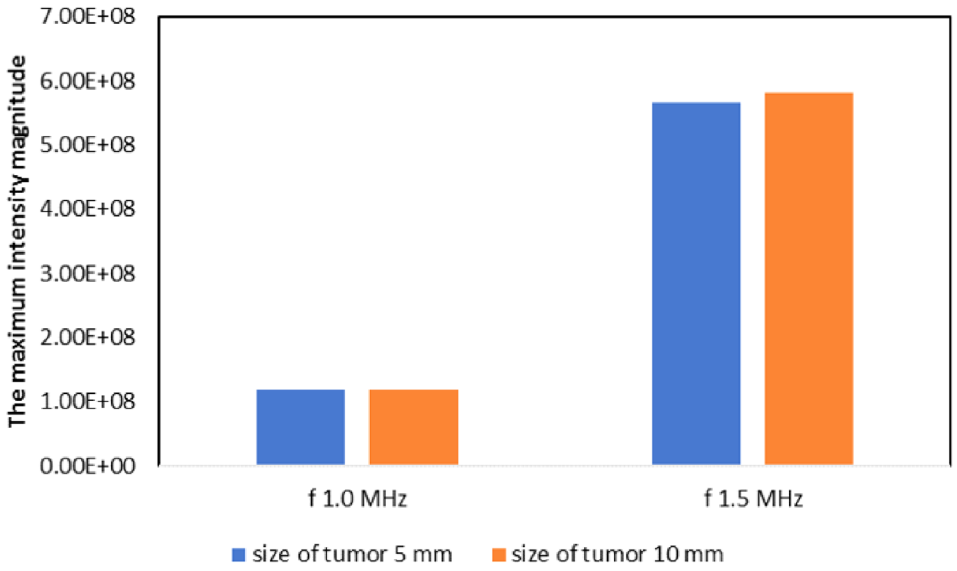

Fig. 8 The bar graph of the maximum intensity magnitude of the different ultrasound frequency (1.0 and 1.5 MHz) and size of tumor (5 and 10 mm) at ablation time of 10 s

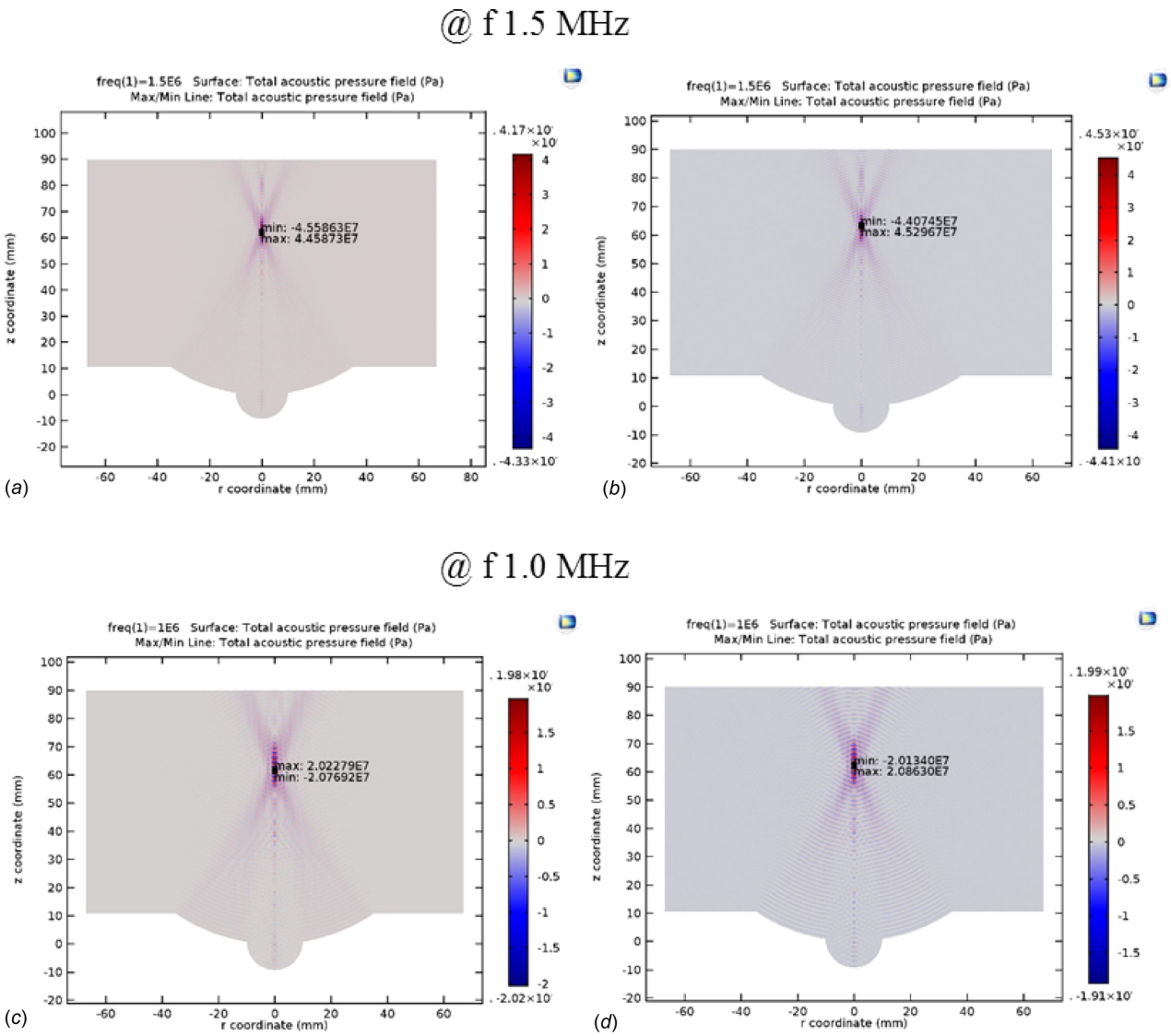

Fig. 9 The total acoustic pressure field in the breast cancer tissue domains at frequency of 1.5 and 1.0 MHz, size of tumor of 5 mm and 10 mm: (*a*) size of tumor 5 mm, f 1.5 MHz, (*b*) size of tumor 10 mm, f 1.5 MHz, (*c*) size of tumor 5 mm, f 1.0 MHz, and (*d*) size of tumor 10 mm, f 1.0 MHz

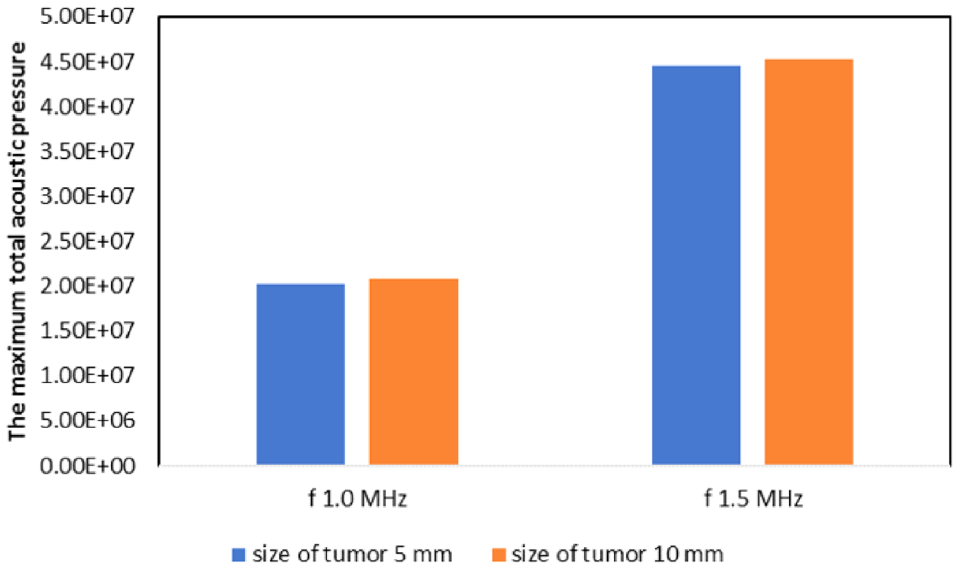

Fig. 10 The bar graph of the maximum total acoustic pressure field of the different ultrasound frequency (1.0 and 1.5 MHz) and size of tumor (5 and 10 mm) at ablation time of 10 s

moves through a soft tissue layer, shearing motion is generated by the induced pressure fluctuations, which results in frictional heating. When an ultrasound wave propagates through inhomogeneous media, the wave is scattered in all directions, due to the small regions with different properties within this media, compared to their surroundings, resulting in a loss in acoustic energy [25,35]. The attenuation coefficient is related to the ultrasound frequency and is therefore in most tissues ideal for the use of noninvasive treatment. However, problems arise when the ultrasound excitation frequency is increased, which causes both the absorption coefficient and the attenuation coefficient to increase, resulting in a higher heat disposition and a lower penetration depth [25,35]. As a result, the optimal treatment frequency is dependent on the application; a compromise is needed between the desired penetration depth and the hyperthermia rate [25,35,36].

When an ultrasound wave propagates linearly through soft tissue, the hyperthermia rate is dependent on the incident ultrasound intensity and the local tissue absorption coefficient. Any nonlinear mechanism that gives rise to higher frequency components in the ultrasound wave will produce enhanced heating due to the frequency dependency of the absorption coefficient previously described. Two mechanisms play an important role in HIFU; nonlinear wave propagation and cavitation [25,37].

In nonlinear wave propagation, the ultrasound wave becomes gradually shocked resulting in energy loss from the excitation frequency to higher frequencies. The extent of this loss is dependent on the amplitude of the incident wave, the nonlinearity of the medium, and the travel distance of the ultrasound wave. The nonlinear effects become more significant in HIFU when there is an increased treatment depth or when a region of high intensity is similar to a region of fatty tissue, which has a higher amount of nonlinearity. In HIFU, the heating observed is contributed to significantly by nonlinear wave propagation [25,26].

High-intensity focused ultrasound (HIFU) therapy has been developed as the noninvasive treatment of deep cancers in particular. Issues as the defocusing and distortion of ultrasound in the body and the long treatment time in current HIFU should be resolved quickly. So, this 2D numerical simulation is required for the early development of the advance HIFU system.

The effects of ultrasound frequency, size of tumor on the temperature distribution, total acoustic pressure, intensity magnitude, and total displacement in deformed breast cancer tissue during focused ultrasound ablation were carried out systematically.

4.1 Verification of the Model. In order to verify the accuracy of the present numerical model, the modified case of the simulated results was then validated and the numerical results with the geometric model under the same conditions were obtained by Bhowmik et al. [1]. The axial symmetry-layered breast tissue model, which comprises fat, glandular, and muscle is simulated with an ultrasound frequency of 1.5 MHz and size of tumor of 5 and 10 mm. The temperature distributions with elapsed times are indicated and compared with the present result in Fig. 6. Overall, the results of this study are in excellent agreement with the analytical results obtained by Bhowmik et al. [1]. This highly favorable comparison lends confidence to the accuracy of the present numerical model. This agreement supports the present numerical model, which is accurate. However, some errors may occur in simulations by acoustic properties, thermal properties, and numerical scheme. This model can be used to describe the fundamental attributes of heat transfer and the total displacement in a breast cancer tissue subjected to an imposed focus ultrasound ablation.

4.2 The Intensity Magnitude and the Acoustic Pressure Field. Wave frequency is an important parameter in therapeutic ultrasound. Ultrasound increases with frequency consequently; high frequency ultrasound is used for imaging and therapy near or at the body surface, while low-frequency ultrasound is appropriate for deeper imaging and therapy [38,39]. Frequency also has an effect on the dimensions of the focal points.

Figure 7 shows the intensity magnitude at size of tumor of 5 mm, frequency of 1.0 MHz and 1.5 MHz with ablation time of 10 s. The maximum intensity magnitude of frequency of 1.0 MHz and 1.5 MHz is 1.1795×10^8 and 5.6767×10^8, respectively, at the focal points, since ultrasound frequency direct variation on intensity magnitude. Figure 8 shows the bar graph maximum intensity magnitude of the different ultrasound frequency (1.0 and 1.5 MHz) and the size of the tumor (5 and 10 mm) at an ablation time of 10 s. The bar graph shows the maximum intensity magnitude of ultrasound frequency of 1.5 MHz is higher than ultrasound frequency of 1.0 MHz. The maximum intensity magnitude of the size of tumor of 10 mm is a little higher than of size of tumor of 5 mm, show that larger size accumulates more intensity magnitude. Figure 9 shows the total acoustic pressure field in the breast cancer tissue domains at frequency of 1.5 and 1.0 MHz, size of

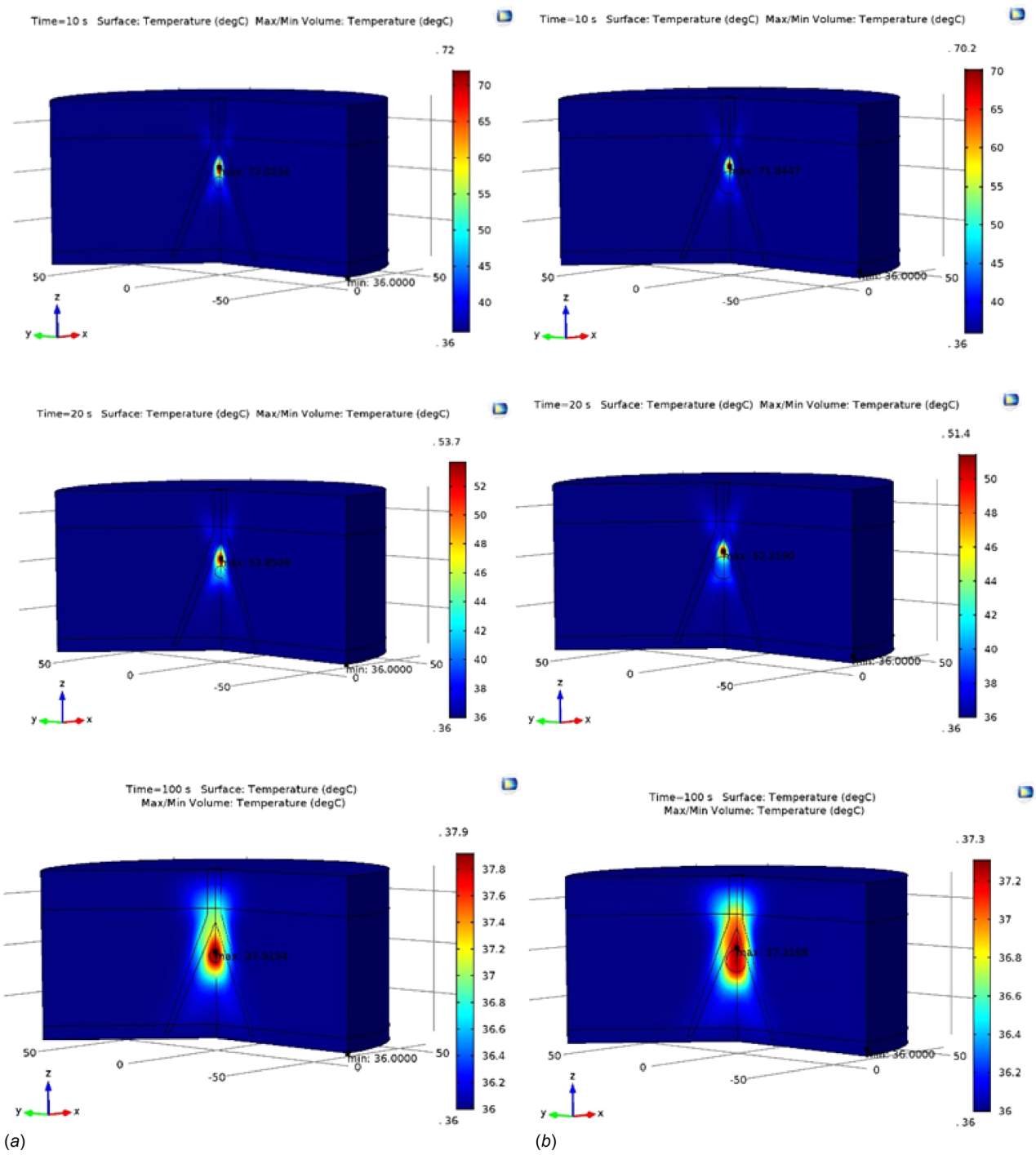

Fig. 11 The temperature distribution at frequency of 1.5 MHz, size of tumor of 5 mm and 10 mm, ultrasound ablation time at 10, 20 and 100 s: (*a*) size of tumor 5 mm and (*b*) size of tumor 10 mm

tumor of 5 mm and 10 mm. (a) size of tumor 5 mm, f 1.5 MHz, (b) size of tumor 10 mm, f 1.5 MHz, (c) size of tumor 5 mm, f 1.0 MHz, (d) size of tumor 10 mm, f 1.0 MHz. The maximum total acoustic pressure field is 4.458×10^{-7}, 4.529×10^{-7}, 2.022×10^{-7}, and 2.086×10^{-7}, respectively. Figure 10 shows the bar graph of the maximum total acoustic pressure field of the different ultrasound frequency (1.0 and 1.5 MHz) and size of tumor (5 and 10 mm) at ablation time of 10 s. From the graph, it can be seen that the maximum total acoustic pressure field of the greater tumor size (10 mm) is a little higher than that of the smaller tumor size (5 mm), and the maximum total acoustic pressure field of ultrasound frequency of 1.5 MHz is higher than that of ultrasound frequency of 1.0 MHz, showing that larger size accumulates more total acoustic pressure field and high ultrasound frequency causes high maximum total acoustic pressure field.

4.3 The Temperature Distribution. In general, the energy of pressure acoustic wave is quite high and causes a significant rise in the local temperature of the targeted tissue and has the

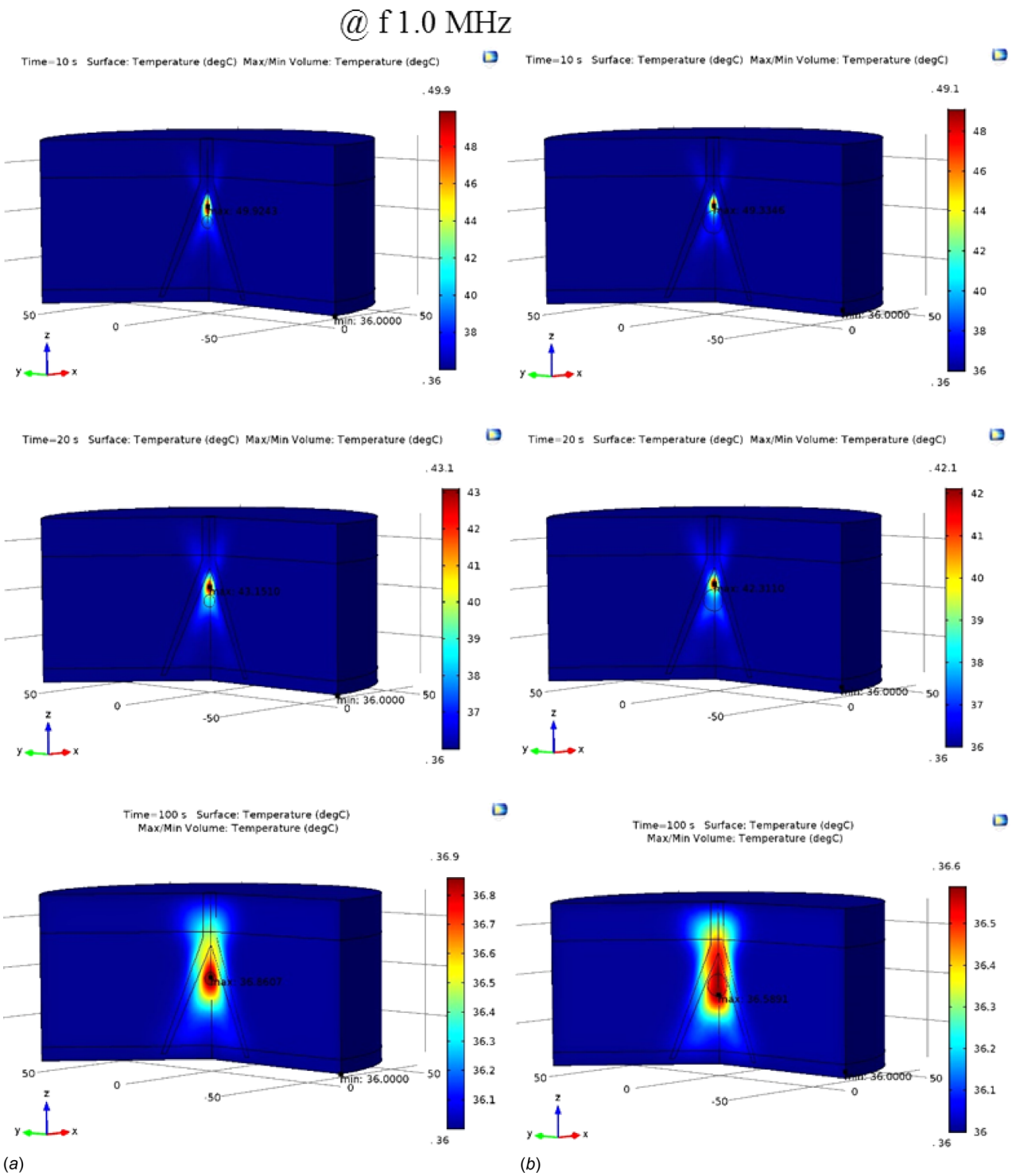

Fig. 12 The temperature distribution at frequency of 1.0 MHz, size of tumor of 5 mm and 10 mm, ultrasound ablation time at 10, 20, and 100 s: (*a*) size of tumor 5 mm and (*b*) size of tumor 10 mm

ability to heat the deep seated tumor selectively. The rise in temperature within breast cancer is a function of physical properties of the medium, configuration of the acoustic device, frequency of ultrasound, exposure time, and the time of ablation.

Figure 11 shows the temperature distribution at frequency of 1.5 MHz, size of tumor of 5 mm and 10 mm, ultrasound ablation time at 10, 20, and 100 s (a) size of tumor 5 mm, f 1.5 MHz, (b) size of tumor 10 mm, f 1.5 MHz. Figure 12 shows the temperature distribution at frequency of 1.0 MHz, size of tumor of 5 mm and 10 mm, ultrasound ablation time at 10, 20 and 100 s (a) Size of tumor 5 mm, f 1.0 MHz, (b) Size of tumor 10 mm, f 1.0 MHz, the maximum temperature distribution at exposure time 10 s at ultrasound frequency of 1.5 and 1.0 MHz is 72.0234 °C and 71.8447 °C, respectively. The higher frequency resulting in higher intensity magnitude caused a higher, more concentrated power deposition.

Figure 13 shows the temperature distribution of the different ultrasound frequency (1.0 and 1.5 MHz) and size of tumor (5 and 10 mm) at the ablation time of 0, 10, 20, 40, 60, 80, and 100 s. See that the temperature changes over time increase from 36 °C until

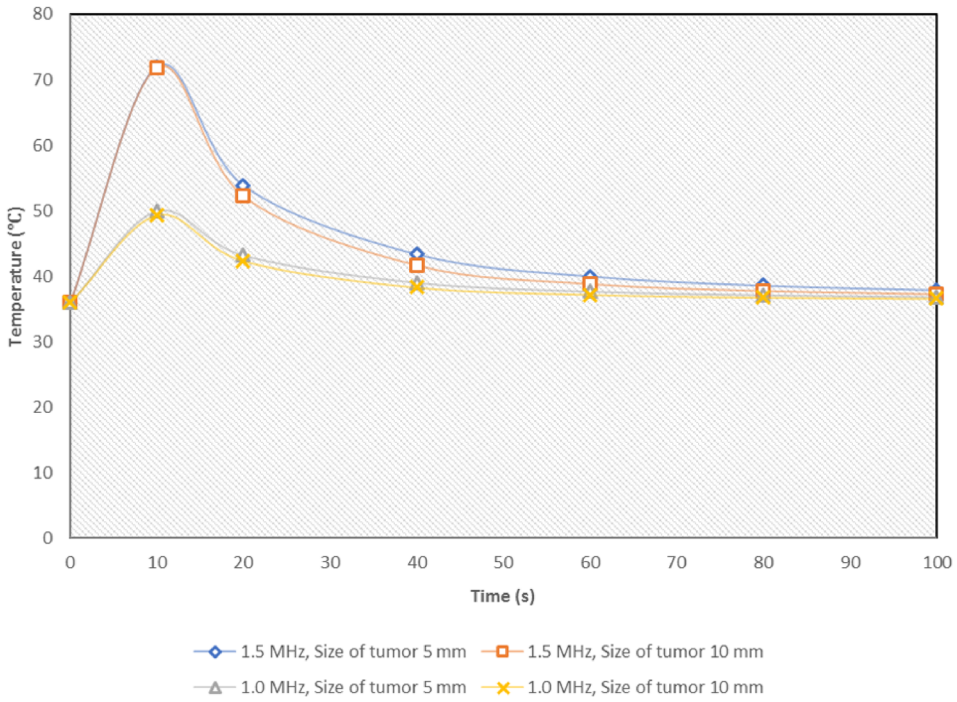

Fig. 13 The temperature distribution of the different ultrasound frequency (1.0 and 1.5 MHz) and size of tumor (5 and 10 mm) at ablation time of 0, 10, 20, 40, 60, 80, and 100 s

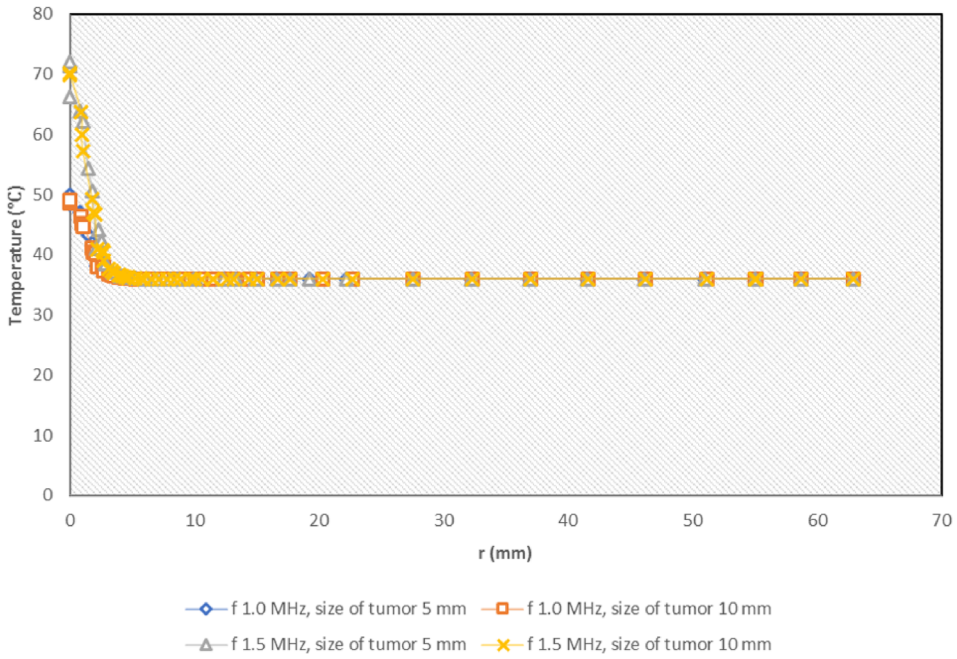

Fig. 14 The temperature distribution along radial direction of the different ultrasound frequency and size of tumor at ablation time of 10 s

71–72 °C at 10 s. Then the temperature gradually decreases over time at 36–37 °C

Figure 14 shows the temperature distribution along radial direction of the different ultrasound frequency and size of tumor at ablation time of 10 s. At r position = 0 mm, the temperature is high and gradually decreases to a temperature of 36 °C and remains constant throughout the radial direction. And at frequency of 1.5 MHz, the temperature is higher than 1 MHz and size of 5 mm of tumor, slightly higher temperature.

Figure 15 shows the temperature distribution along the longitudinal direction of the different ultrasound frequency and size of tumor at ablation time of 10 s. See that the frequency has the greatest effect on temperature. At frequency 1.5 MHz and the size of tumor smaller get better temperature distribution. The maximum temperature distribution around 72 °C at along the longitudinal direction = 62–63 mm because it is the focal point where the focal length of transducer (5.5 cm) is the distance from the tumor.

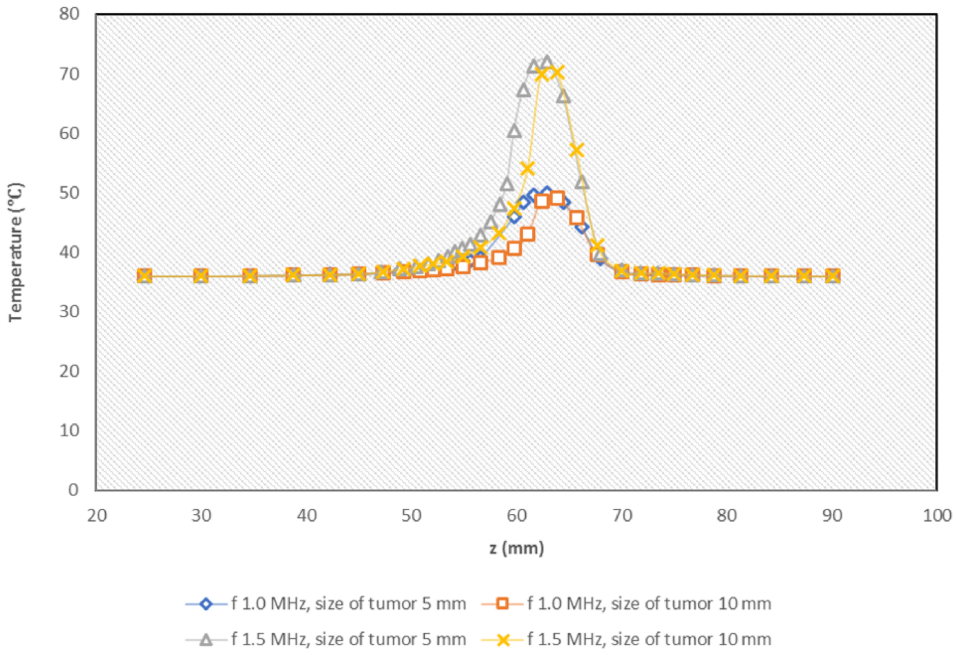

Fig. 15 The temperature distribution along longitudinal direction of the different ultrasound frequency and size of tumor at ablation time of 10 s

@ f 1.5 MHz

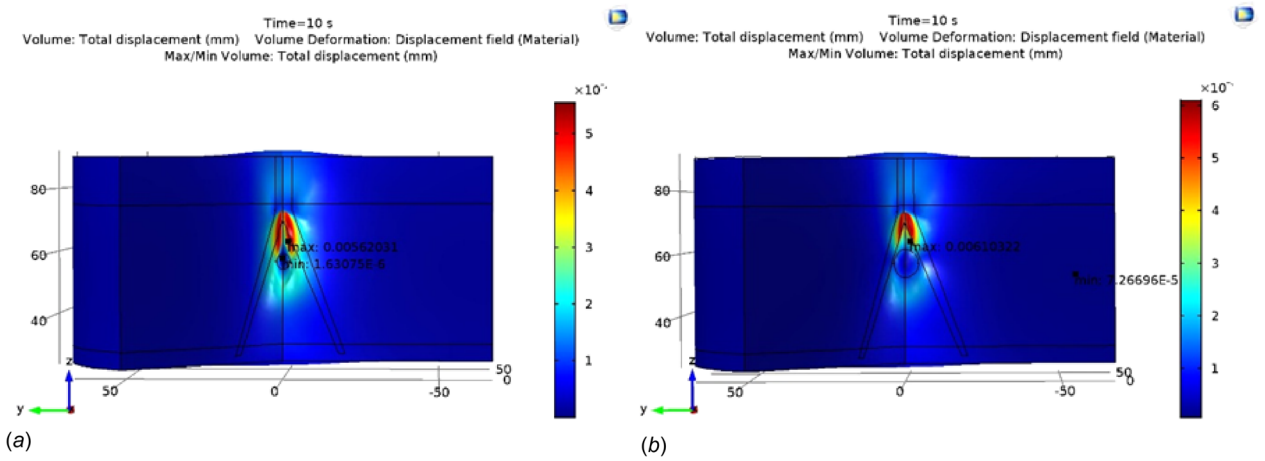

@ f 1.0 MHz

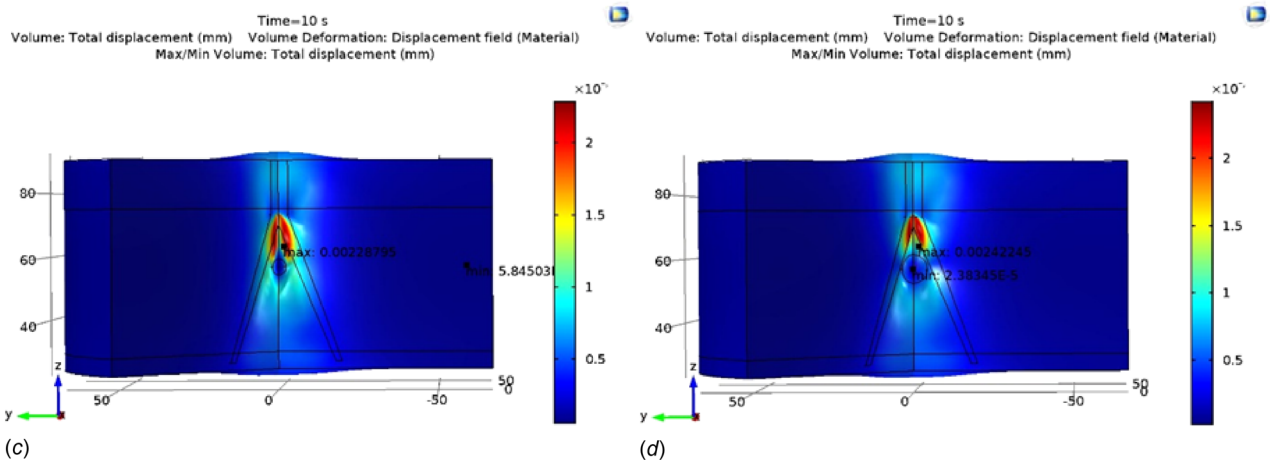

Fig. 16 The 3D total displacement field at frequencies of 1.5 and 1.0 MHz and, size of tumor 5 and 10 mm at ablation time 10 s: (*a*) size of tumor 5 mm, f 1.5 MHz, (*b*) size of tumor 10 mm, f 1.5 MHz, (*c*) size of tumor 5 mm, f 1.0 MHz, and (*d*) size of tumor 10 mm, f 1.0 MHz

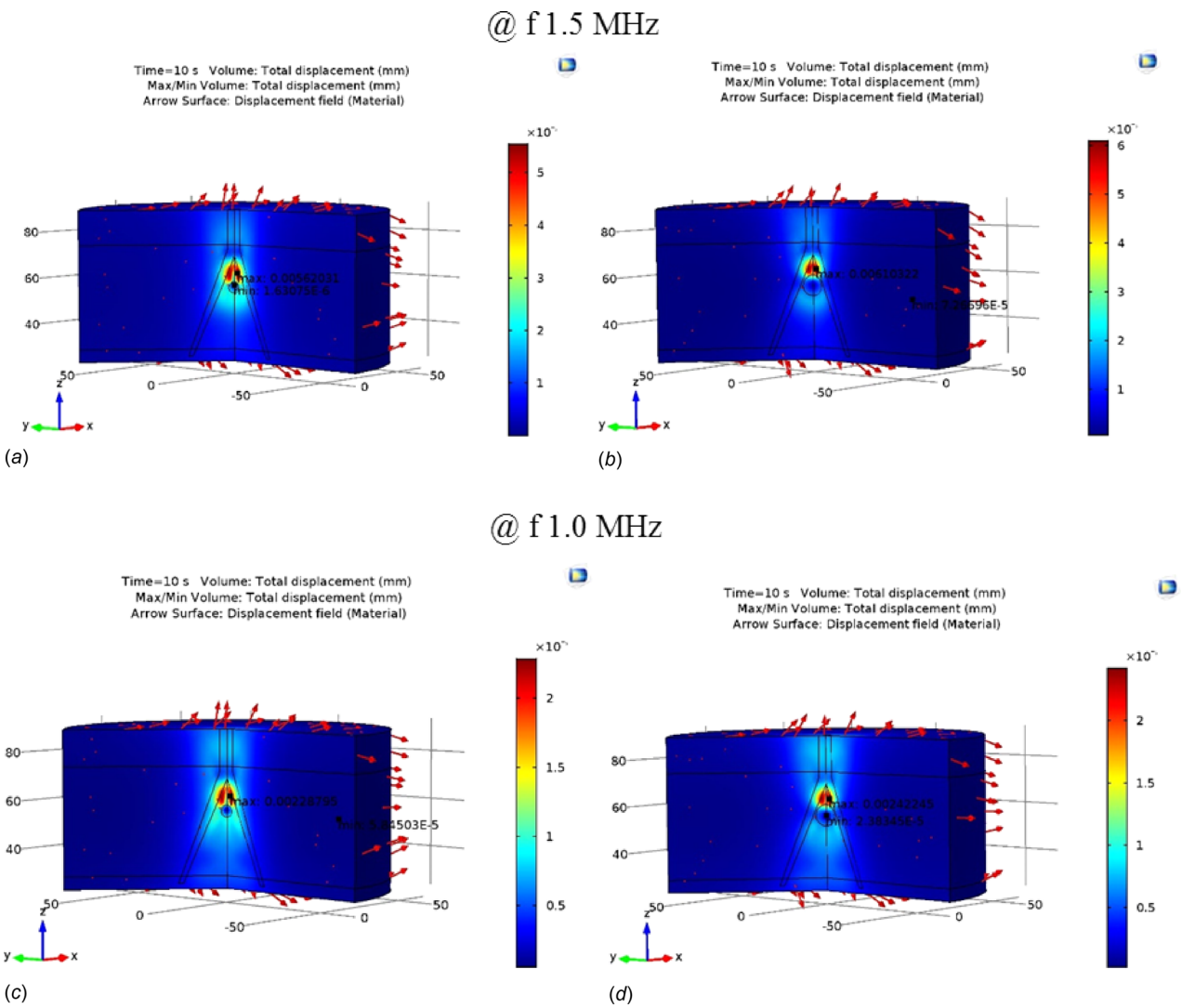

Fig. 17 The 3D total displacement with arrow direction at frequencies of 1.5 and 1.0 MHz and, size of tumor 5 and mm at ablation time 10 s: (*a*) size of tumor 5 mm, f 1.5 MHz, (*b*) size of tumor 10 mm, f 1.5 MHz, (*c*) size of tumor 5 mm, f 1.0 MHz, and (*d*) size of tumor 10 mm, f 1.0 MHz

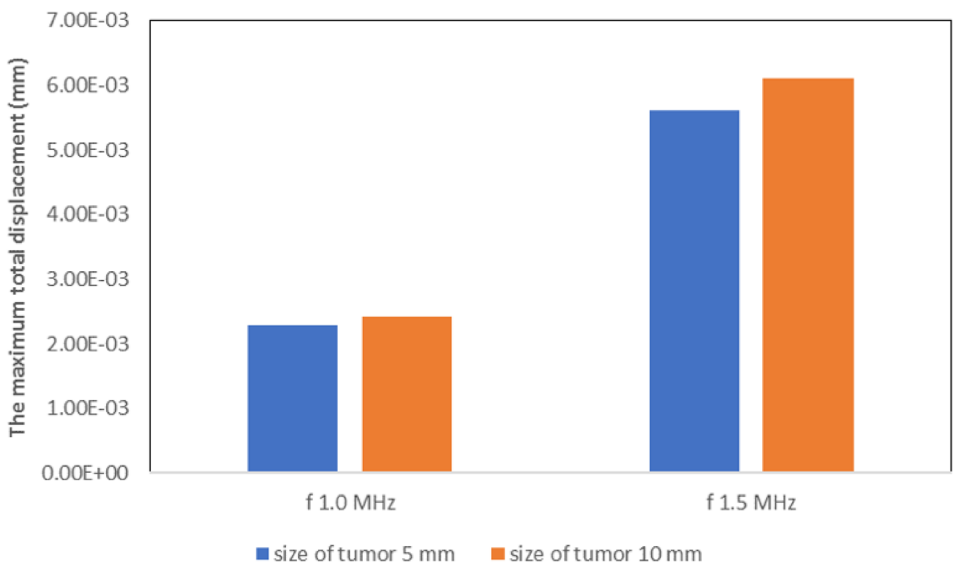

Fig. 18 The bar graph of the maximum total displacement of the different ultrasound frequency (1.0 and 1.5 MHz) and size of tumor (5 and 10 mm) at ablation time of 10 s

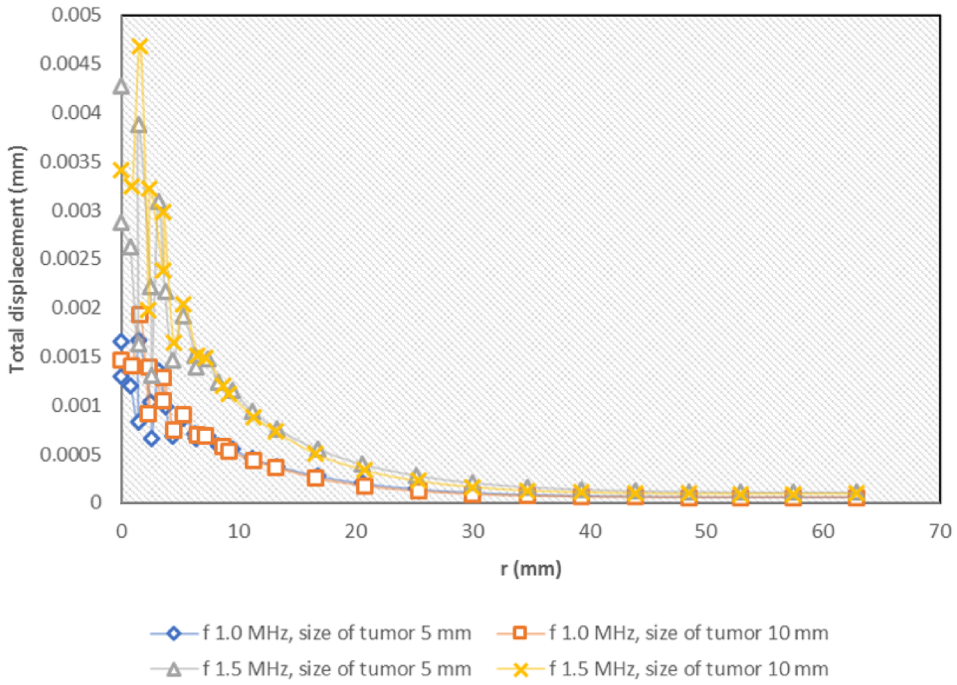

Fig. 19 The total displacement along radial direction of the different ultrasound frequency and size of tumor at ablation time of 10 s ($z = 65–66$)

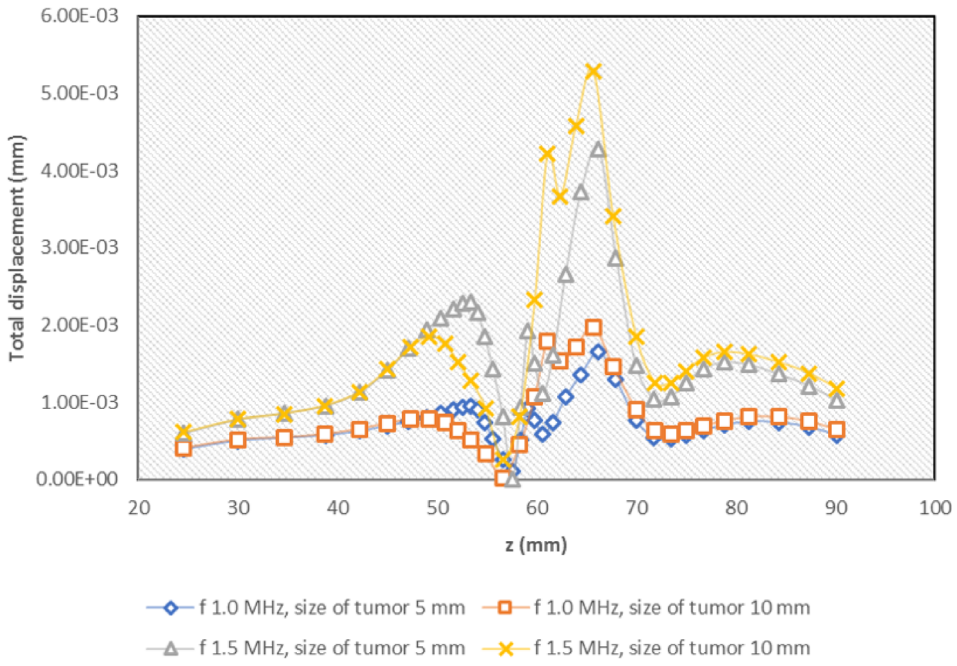

Fig. 20 The total displacement along longitudinal direction of the different ultrasound frequency and size of tumor at ablation time of 10 s ($r = 0$ mm)

Therefore, HIFU therapy can transport energy in the form of waves through a media of intervening tissues to specific target points of body organs, and hence, increase the temperature or bring about other biological interactions in an absolutely noninvasive manner.

4.4 The Total Displacement Distribution. Effect of ultrasound frequency and size of tumor to the total displacement distribution are shown in Figs. 16–20. Figure 16 shows the 3D total displacement field at difference frequency and, difference size of tumor at ablation time 10 s. It can be seen that the total displacement of the greater tumor size (10 mm) is higher than that of the smaller tumor size (5 mm).

The 3D total displacement with arrow direction at frequencies of 1.5 and 1.0 MHz shows that the arrow direction in all cases has same direction and the maximum total displacement is on the focal points of the breast tissue model, namely, the position of the maximum total displacement does not change that shown in Fig. 17.

Figure 18 shows the bar graph of the maximum total displacement of the different ultrasound frequency (1.0 and 1.5 MHz) and

the size of the tumor (5 and 10 mm) at an ablation time of 10 s. The maximum total displacement of ultrasound frequency of 1.5 MHz is higher than ultrasound frequency of 1.0 MHz and the maximum total displacement of the size of tumor of 10 mm is a little higher than of size of tumor of 5 mm because the large size of the tumor can receive more heat and engender high maximum total displacement. It shows that when breast tissue is exposed to ultrasound ablation at the same ultrasound frequency of 1.5 MHz, size of tumor of 10 mm causes tissue to expand more than size of tumor of 5 mm.

From the 3D total displacement, we can plot the total displacement along radial direction and longitudinal direction shown in Figs. 19 and 20. Figure 19 shows the total displacement along radial direction of the different ultrasound frequencies (1.0 and 1.5 MHz), and the different size of tumor (5 and 10 mm) at ablation time of 10 s. The total displacement is highest in the first period and swing after that gradually decrease and be constant at along radial direction $r = 35$ mm. Figure 20 shows the total displacement along the longitudinal direction of the different ultrasound frequencies (1.0 and 1.5 MHz), and the different size of tumor (5 and 10 mm) at ablation time of 10 s. The total displacement is gradually increased and is decreased lowest at $z = 58$ mm and swings up and down then the total displacement has highest at longitudinal direction $z = 65$–66 mm. After that, the total displacement dropping again to the longitudinal direction z about 73 mm, and shows that after $z = 58$ mm, the size of tumor 10 mm is more the total displacement than the size of tumor 5 mm tumor, where it is a region of focal points.

Effect of the size of tumor to the total displacement distribution as follows, Fig. 19 shows that at first, the total displacement is slightly different at the size of tumor 5 mm and 10 mm and same ultrasound frequency. After that at the radial direction $r = 5$ mm onward, the total displacement of the size of tumor 5 and 10 mm is nearby. Figure 20 shows that at first, the total displacement has the same value of the total displacement at the size of tumor 5 mm and 10 mm and same ultrasound frequency until the longitudinal direction $z = 50$ mm, then the total displacement of the size of tumor 5 mm is more than 10 mm. After that, at the longitudinal direction $z = 60$, the total displacement of the size of tumor 10 mm is more than 5 mm where it is a region of focal points. And the longitudinal direction $z = 65$–66 onward, the total displacements of the size of tumors 5 and 10 mm are similar again.

5 Conclusions

Computer simulation is necessary to improve the ultrasound ablation procedure. A method that leads to accurately lesion size control is needed for the clinical treatment with ultrasound ablation in order to guarantee destruction of the breast cancer tissue and minimizing damage to surrounding healthy tissue. This research is carried out to observe the effects of size of tumor and frequency of ultrasound on the temperature distribution, the maximum total acoustic pressure, the maximum intensity magnitude, and the maximum total displacement in breast cancer tissue during ultrasound ablation. The results obtained accurately represent the phenomena occurring in the breast cancer tissue during the ultrasound ablation. The temperature distribution, the total acoustic pressure, the intensity magnitude, and the total displacement have a slightly different for various tumor sizes. The tumor size has only a small effect on the temperature distribution, the total acoustic pressure, the intensity magnitude, and the total displacement. In addition, greater input ultrasound frequency leads to a higher temperature distribution, the total acoustic pressure, the intensity magnitude, and the total displacement; it can be seen that the total acoustic pressure and the intensity magnitude resulted in increasing the temperature distribution within the breast cancer tissue. The present ultrasound ablation model is examined for advancing the transport phenomena in biomedical applications. This study predicts the heating of breast cancer tissue, provides high-performance ultrasound treatment, and does not affect the surrounding tissues

5.1 Significant of This Work. This study presents the numerical analysis of heat transfer in localized deformed breast cancer model exposed to ultrasound ablation. The mathematical model combining Pennes' bioheat equation, heat transfer, and momentum in blood vessel and pressure acoustic is used for all cases. The obtained results contribute to the understanding of the effect of related parameters to reducing side effect from hyperthermal and preplanning in practical application. Parametric studies on thermal enhanced effects for the ultrasound ablation in five types of tissues (fat, glandular, muscle, blood vessel, and the tumor) by varying the parameters of ultrasound frequency, and size of tumor for achieving an optimum condition for breast cancer treatment by high intensity focused ultrasound.

Acknowledgment

The Thailand Government Budget Grant provided financial support for this study.

Funding Data

- Thailand Research Fund (TRF) under the Royal Golden Jubilee Ph.D. Program (RGJ) contract No. PHD/0059/2557, RTA 5980009 (Funder ID: 10.13039/501100004396).

Nomenclature

C = specific heat capacity (J/(kg K))
f = frequency (MHz)
F = body force
k = thermal conductivity (W/(m K))
n = normal vector
p = pressure (N/m^2)
Q = heat source (W/m^3)
t = time (s)
T = tissue temperature (K)
u = velocity (m/s)
ε = strain (Pa)
μ = dynamic viscosity (m^2/s)
ρ = density (kg/m^3)
σ = stress (Pa)
ω = angular frequency $= 2\pi f$ (rad/s)

Subscripts

am = ambient
b = blood
eq = equilibrium
ext = external
$i, r.z, \varphi$ = relative
met = metabolic
ref = reference
0 = free space, initial condition

References

[1] Bhowmik, A., Repaka, R., Mishra, S. C., and Mitra, K., 2015, "Thermal Assessment of Ablation Limit of Subsurface Tumor During Focused Ultrasound and Laser Heating," ASME J. Therm. Sci. Eng. Appl., **8**(1), p. 011012.
[2] Cancer Fact Sheets, 2012, "GLOBOCAN 2012: Estimated Cancer Incidence, Mortality and Prevalence Worldwide in 2012," Cancer Today - IARC, Lyon, France, accessed Apr. 4, 2014, http://globocan.iarc.fr/Pages/fact_sheets_cancer.aspx
[3] Kennedy, J. E., 2005, "High-Intensity Focused Ultrasound in the Treatment of Solid Tumours," Nat. Rev. Cancer, **5**(4), pp. 321–327.
[4] Wu, F., Wang, Z.-B., Chen, W.-Z., Zou, J.-Z., Bai, J., Zhu, H., Li, K.-Q., Xie, F.-L., Jin, C.-B., Su, H.-B., and Gao, G.-W., 2004, "Extracorporeal Focused Ultrasound Surgery for Treatment of Human Solid Carcinomas: Early Chinese Clinical Experience," Ultrasound Med. Biol., **30**(2), pp. 245–260.

[5] Hadjiargyrou, M., McLeod, K., Ryaby, J. P., and Rubin, C., 1998, "Enhancement of Fracture Healing by Low Intensity Ultrasound," Clin. Orthop. Relat. Res., **355**, pp. S216–S229.
[6] Postema, M., and Gilja, O. H., 2007, "Ultrasound-Directed Drug Delivery," Curr. Pharm. Biotechnol., **8**(6), pp. 355–361.
[7] Tachibana, K., and Tachibana, S., 2001, "The Use of Ultrasound for Drug Delivery," Echocardiography, **18**(4), pp. 323–328.
[8] Hynynen, K., and Davis, K. L., 1993, "Small Cylindrical Ultrasound Sources for Induction of Hyperthermia Via Body Cavities or Interstitial Implants," Int. J. Hyp., **9**(2), pp. 263–274.
[9] Hurwitz, M. D., Kaplan, I. D., Svensson, G. K., Hansen, M. S., and Hynynen, K., 2001, "Feasibility and Patient Tolerance of a Novel Transrectal Ultrasound Hyperthermia System for Treatment of Prostate Cancer," Int. J. Hyp., **17**(1), pp. 31–37.
[10] Hynynen, K., and Deyoung, D., 1988, "Temperature Elevation at Muscle-Bone Interface During Scanned, Focused Ultrasound Hyperthermia," Int. J. Hyp., **4**(3), pp. 267–279.
[11] Lawrie, A., Brisken, A., Francis, A., Tayler, D., Chamberlain, J., Crossman, D., Cumberland, D., and Newman, C., 1999, "Ultrasound Enhances Reporter Gene Expression After Transfection of Vascular Cells In Vitro," Circulation, **99**(20), pp. 2617–2620.
[12] Ter Haar, G., 2012, "Ultrasound Mediated Drug Delivery, a 21st Century Phoenix," Int. J. Hyperthermia, Official J. Eur. Soc. Hyperthermic Oncol., North Am. Hyperthermia Group, **28**(4), p. 279.
[13] Seufi, A. M., Ibrahim, S. S., Elmaghraby, T. K., and Hafez, E. E., 2009, "Preventive Effect of the Flavonoid, Quercetin, on Hepatic Cancer in Rats Via Oxidant/Antioxidant Activity: Molecular and Histological Evidences," J. Exp. Clin. Cancer Res., **28**(1), p. 80.
[14] Yang, D., Converse, M. C., Mahvi, D. M., and Webster, J. G., 2007, "Measurement and Analysis of Tissue Temperature During Microwave Liver Ablation," IEEE Trans. Biomed. Eng., **54**(1), pp. 150–155.
[15] Montienthong, P., Rattanadecho, P., and Klinbun, W., 2017, "Effect of Electromagnetic Field on Distribution of Temperature, Velocity and Concentration During Saturated Flow in Porous Media Based on Local Thermal Non-Equilibrium Models (Influent of Input Power and Input Velocity)," Int. J. Heat Mass Transfer, **106**, pp. 720–730.
[16] Wessapan, T., and Rattanadecho, P., 2012, "Numerical Analysis of Specific Absorption Rate and Heat Transfer in Human Head Subjected to Mobile Phone Radiation: Effects of User Age and Radiated Power," ASME J. Heat Transfer, **134**(12), p. 121101.
[17] Klinbun, W., and Rattanadecho, P., 2012, "Numerical Model of Microwave Driven Convection in Multi-Layer Porous Pack Bed Using a Rectangular," ASME J. Heat Transfer, **134**(4), p. 042605.
[18] Wessapan, T., and Rattanadecho, P., 2012, "Specific Absorption Rate and Temperature Increase in Human Eye Subjected to Electromagnetic Fields at 900 MHz," ASME J. Heat Transfer, **134**(9), p. 091101.
[19] Wessapan, T., Srisawatdhisukul, S., and Rattanadecho, P., 2011, "Numerical Analysis of Specific Absorption Rate and Heat Transfer in the Human Body Exposed to Leakage Microwave Power at 915 MHz and 2,450 MHz," ASME J. Heat Transfer, **133**(5), p. 051101.
[20] Wongchadakul, P., Rattanadecho, P., and Wessapan, T., 2018, "Implementation of a Thermomechanical Model to Simulate Laser Heating in Shrinkage Tissue (Effects of Wavelength, Laser Irradiation Intensity, and Irradiation Beam Area)," Int. J. Therm. Sci., **134**, pp. 321–336.
[21] Manenti, G., Scarano, A. L., Pistolese, C. A., Perretta, T., Bonanno, E., Orlandi, A., and Simonetti, G., 2013, "Subclinical Breast Cancer: Minimally Invasive Approaches. Our Experience With Percutaneous Radiofrequency Ablation vs. Cryotherapy," Breast Care (Basel)., **8**(5), pp. 356–360.
[22] Quaranta, V., Manenti, G., Bolacchi, F., Cossu, E., Pistolese, C. A., Buonomo, O. C., Carotenuto, L., Piconi, C., and Simonetti, G., 2007, "FEM Analysis of RF Breast Ablation: Multiprobe Versus Cool-Tip Electrode," Anticancer Res., **27**, pp. 775–784.
[23] Hipp, E., Partanen, A., Karczmar, G. S., and Fan, X., 2012, "Safety Limitations of MR-HIFU Treatment Near Interfaces: A Phantom Validation," J. Appl. Clin. Med. Phys., **13**(2), p. 3739.
[24] Yang, R., Reilly, C. R., Rescorla, F. J., Sanghvi, N. T., Fry, F. J., Franklin, T. D., and Grosfeld, J. L., 1992, "Effects of High-Intensity Focused Ultrasound in the Treatment of Experimental Neuroblastoma," J. Pediatr. Surg., **27**(2), pp. 246–251.
[25] Haar, G. T., and Coussios, C., 2007, "High Intensity Focused Ultrasound: Physical Principles and Devices," Int. J. Hyperthermia., **23**(2), pp. 89–104.
[26] Dubinsky, T. J., Cuevas, C., Dighe, M. K., Kolokythas, O., and Hwang, J. H., 2008, "High-Intensity Focused Ultrasound: Current Potential and Oncologic Applications," Am. J. Roentgenol., **190**(1), pp. 191–199.
[27] Huang, J., Holt, R. G., Cleveland, R. O., and Roy, R. A., 2004, "Experimental Validation of a Tractable Numerical Model for Focused Ultrasound Heating in Flow-Through Tissue Phantoms," J. Acoust. Soc. Am., **116**(4 Pt. 1), pp. 2451–2458.
[28] Wulff, W., 1974, "The Energy Conservation Equation for Living Tissue," IEEE Trans. Biomed. Eng., **21**(6), pp. 494–495.
[29] Klinger, H. G., 1974, "Heat Transfer in Perfused Biological Tissue—I: General Theory," Bull. Math. Biol., **36**(4), pp. 403–415.
[30] Chen, M. M., and Holmes, K. R., 1980, "Microvascular Contributions in Tissue Heat Transfer," Ann. N. Y. Acad. Sci., **335**, pp. 137–150.
[31] Pennes, H. H., 1948, "Analysis of Tissue and Arterial Blood Temperature in the Resting Human Forearm," J. Appl. Physiol., **1**(2), pp. 93–122.
[32] Pennes, H. H., 1998, "Analysis of Tissue and Arterial Blood Temperatures in the Resting Human Forearm," J. Appl. Phys., **85**, pp. 5–34.
[33] Saladin, K. S., 2011, *Anatomy and Physiology: The Unity of Form and Function*, 6th ed., McGraw-Hill, New York, pp. 678–749.
[34] White, P. J., Clement, G. T., and Hynynen, K., 2006, "Local Frequency Dependence in Transcranial Ultrasound Transmission," Phys. Med. Biol., **51**(9), pp. 2293–2305.
[35] Thanou, M., and Gedroyc, W., 2013, "MRI-Guided Focused Ultrasound as a New Method of Drug Delivery," J. Drug Deliv., **2013**, p. 616197.
[36] Hill, C. R., 1994, "Optimum Acoustic Frequency for Focused Ultrasound Surgery," Ultrasound Med. Biol., **20**(3), pp. 271–277.
[37] Zderic, V., Keshavarzi, A., Andrew, M. A., Vaezy, S., and Martin, R. W., 2004, "Attenuation of Porcine Tissues In Vivo After High-Intensity Ultrasound Treatment," Ultrasound Med. Biol., **30**(1), pp. 61–66.
[38] Daftari, I., Barash, D., Lin, S., and O'Brien, J., 2001, "Use of High-Frequency Ultrasound Imaging to Improve Delineation of Anterior Uveal Melanoma for Proton Irradiation," Phys. Med. Biol., **46**(2), pp. 579–590.
[39] Chen, L., Dyson, M., Rymer, J., Bolton, P., and Young, S., 2001, "The Use of High-Frequency Diagnostic Ultrasound to Investigate the Effect of Hormone Replacement Therapy on Skin Thickness," Skin Res. Technol., **7**(2), pp. 95–97.